Combustion and Flame 219 (2020) 478–487

Contents lists available at ScienceDirect

Combustion and Flame

journal homepage: www.elsevier.com/locate/combustflame

New coordination complexes-based gas-generating energetic composites

Tao Wu[a], Florent Sevely[a], Baptiste Julien[a], Felipe Sodre[a], Jeremy Cure[a], Christophe Tenailleau[b], Alain Esteve[a], Carole Rossi[a,*]

[a] LAAS-CNRS, University of Toulouse, 7 Avenue du colonel Roche, 31400 Toulouse, France
[b] CIRIMAT, University of Toulouse, CNRS, UT3-Paul Sabatier, 118 route de Narbonne, 31062 Toulouse, France

ARTICLE INFO

Article history:
Received 6 April 2020
Revised 27 May 2020
Accepted 27 May 2020

Keywords:
Coordination complex
Energetic materials
Non-toxic gas generator
Flame propagation
Airbag

ABSTRACT

To reduce the size inconvenience of airbag systems employed in human-body protection devices while maintaining comparable gas generation performance, a new family of gas-generating energetic composites are proposed mixing Al/CuO nanothermite with copper complex ($Cu(NH_3)_4(NO_3)_2$) known for its propensity to generate gases (0.03 mol/g) such as N_2, O_2, N_2O through exothermic chemical decomposition (300 J/g). The aluminum (Al)/Copper oxide (CuO) couple, known as the most widely studied nanomaterial for thermite reactions, releasing a high energy, mostly heat, through chemical reaction, is employed as a source of heat to trigger and sustain the decomposition of $Cu(NH_3)_4(NO_3)_2$ complex. This work permits developing a new family of gas-generating energetic composites that takes advantage of specific chemical and thermal properties of both materials. We demonstrate its capability to tune the pressurization rate, burn rate and pressure peak by varying the Al/CuO over $Cu(NH_3)(NO_2)_2$ mass ratio. The peak pressure of $Cu(NH_3)_4(NO_3)_2$/Al/CuO energetic composites reaches 12 MPa/g.cm^3 in a close volume, which is 3.3 higher than that of traditional Al/CuO nanothermite. They achieve much longer high-pressure duration (~30 ms). They also exhibit very intense burning with velocity reaching hundreds of m/s in opening burning experiments. These new materials appear very promising for green gas generation.

1. Introduction

Automobile airbag systems are the widespread micro-pyrotechnical systems introduced in the earlies 1970s [1] designed to slow down the movement of the car occupants within milliseconds to prevent injury during a collision [2,3]. Recently, new applicative markets have emerged with the goal to prevent personal injuries during extreme sport (skiing, equitation, motorcycling), urban two-wheelers or to protect the elderly from hips fracture when falling. For these new applicative domains, smart inflatable protection devices using compressed CO_2 bottles are now available on the market [4–6]. When the sensors detect a fall, the integrated circuitry triggers the actuator, which then inflates the nylon airbag before the impact [7,8]. However, all commercialized inflator systems are bulky (50–250 cm^3), heavy (more than 1 kg), costly, owing to the fact that a tank with compressed gas is employed to perform the actuation.

Alternatively, gas-generating energetic materials could effectively provide high-energy and high-power actuation within a reduced volume (<50 cm^3) thanks to the large amount of stored chemical energy they can release quickly. In the context of personal protection, they have to meet severe requirements including good performances, moderate temperature (<300°C) [9,10], non-toxicity of gaseous species, reliability [11], safety when handling and during storage, and low energy ignitions. Gas-generating mixtures developed for automobile airbag inflation are mostly based on a propellant, such as sodium azide (NaN_3) and potassium nitrate (KNO_3) that thermally decomposes into gases and residues when they are ignited and they have been used for a long time [12]. A series of chemical reactions produce N_2 to fill the airbag and convert metallic azide which is highly toxic [13] even after reaction due to incomplete combustion. To reduce the toxicity, high nitrogen nonazide gas compositions are proposed and used in inflating passenger restraint gas inflator bags, where ammounium nitrate, guanidine nitrate, etc, are employed [14,15]. However, guanidine compound is explosive from friction and therefore difficult to handle [16]. In fact, ammonium nitrate was used as a gas generator to inflate airbags since 2001 by Takata; however, more than 16 million vehicles were recalled worldwide due to a serious safety issue that high moisture may accelerate the decomposition of ammonium nitrate and leads to violent explosion of the airbags [17,18].

* Corresponding author.
E-mail address: rossi@laas.fr (C. Rossi).

https://doi.org/10.1016/j.combustflame.2020.05.022
0010-2180/

Herein, we consider a new, safe and non-toxic gas-generating materials based on the Werner type complexes composed of a metallic cation (Cu, Fe, Co or Mn) bounded to oxidizing anion ligands (NO^-, NO_3^-, NO_2^-). Numerous complexes have been successfully synthesized and studied by numerous groups such as $Cu(NH_3)_4(NO_3)_2$ [19–22], $Co(NH_3)_6(NO_3))_2$ [23,24], $Mg(NH_3)_6(NO_3)_2$ [25,26], $Ni(NH_3)_6(NO_3)_2$ [25], $Cd(NH_3)_6(NO_3)_2$ [27], because they are stable and enable the generation of abundant environmental friendly gases (N_2, O_2, N_2O) [28] from the thermal decomposition of the organic anion at moderate temperature (150–220°C). In addition, complex compounds usually contain fuel (ligands such as ammonia or nitrogen compounds), oxidizer (like nitrates or perchlorate) and metal that may act as burn modifier.

Among all published coordination complexes, the most studied is $Cu(NH_3)_4(NO_3)_2$ (called CuC) because of its low decomposition temperature and relatively easy synthesis process. Despite a patent that proposes to use a heterometallic Werner complex as a green gas source for airbag application [29], the applicative interest of CuC as a gas-generating material remains stalled since its exothermic decomposition is not a self-sustained process, which means that the entire mass of the complex has to be heated to its decomposition temperature to release the gases requiring a too important external source of heat [20].

This study proposes to incorporate nanothermites into the CuC mixture, to serve as an embedded source of heat to drastically reduce the external activation energy needed to decompose the complex [11]. In contrast to the coordination complex initiation mode, the nanothermite engages a self-sustained reaction upon hot point initiation. In other words, after being ignited locally, the nanothermite is capable of producing enough heat to quickly and entirely heat up the mass of CuC to its decomposition temperature, which decomposition leads to gas release and pressure.

By varying the mass of nanothermite incorporated into the CuC, this study seeks to experimentally find the optimized Al/CuO to CuC mass ratio allowing: (i) the lowering of the power density budget for initiation, (ii) the self-sustained and total decomposition of CuC to maximize the pressure peak, (iii) providing fundamental understanding on the interplay of the two materials. We will discuss the combustion events in such CuC/Al/CuO energetic composites, experimentally evidenced thanks to coupled thermochemical analyses using calorimetry coupled with time-resolved mass spectrometry. Overall, we believe this work opens new perspectives in the field of non-toxic gas generating material for micro and mini-airbag applications since this new energetic composites feature peak pressure of 12 MPa/g per cm^3, which is 3.3 higher than that of traditional Al/CuO nanothermites, with much longer high-pressure durations (~30 ms), and with the production of safe gases only.

2. Experimental Section

2.1. Materials

The aluminum nanopowders (Al) (80 nm) were purchased from Novacentrix and stored in a glove box. The active Al content was 69% by mass, calculated from thermogravimetric analysis before use. Copper oxide (~100 nm), copper nitrate trihydrate and 25% aqueous ammonia, purchased from Sigma-Aldrich were directly used as received.

2.2. Synthesis of CuC

The Cu complex was synthesized according to the literature [21,22]. In brief, 4.83 g (0.02 mol) of copper nitrate trihydrate was dissolved in 10 mL of distilled water followed by addition of 15 mL of 25% aqueous ammonia solution (0.24 mol). The mixed solution was kept in an ice bath with moderate stirring for one hour and then without stirring for three hours. The final product was separated via vacuum filtration and dried in an oven at 70°C. The yield of the product is ~65% (3.2 g).

The X-Ray Diffractometer (XRD) pattern of as-prepared CuC is well correlated to a published $Cu(NH_3)_4(NO_3)_2$ crystal structure with a pdf#01-070-195. A very small trace of $Cu_2(NO_3)(OH)$ was also detected in the mixture (labeled in blue in Supplementary Information Fig. S1A). The FTIR spectrum of synthesized copper complex (Fig. S1B) have the same characteristic peaks as to the literature [21]. Both XRD and FTIR results prove that copper complex was successfully synthesized in this work.

Scanning Electron Microscopy (SEM) was employed to characterize the copper complex particles and the results shown in Supplementary Information Fig. S2 indicate that they are irregularly cylindrical with an average size about 20 µm in width and 60 µm in length. A zoom-in image also shows that the surface of particles is rough, which could be beneficial for further deposition of other materials.

Table 1
Chemical composition of the different batches of CuC/Al/CuO energetic composites

Samples	Al (mg)	CuO (mg)	CuC (mg)	Al/CuO (mg)	Al/CuC (mg)	Total (mg)
Al/CuO	114	286		400		400
Al/CuC	40		360		400	400
CuC/Al/CuO_25	59	71	270	100	300	400
CuC/Al/CuO_50	77	143	180	200	200	400
CuC/Al/CuO_62	86	177	137	248	152	400
CuC/Al/CuO_75	96	214	90	300	100	400
CuC/Al/CuO_82	101	234	65	328	72	400
CuC/Al/CuO_90	107	257	36	360	40	400
CuC/Al/CuO_95	111	271	18	380	20	400

2.3. Preparation of Al/CuC energetic composites

Mixtures of Al/CuC were prepared using a classic sonication method where Al nanoparticles were mixed with CuC with an Al/CuC equivalence ratio of 1.2 in hexane followed by 20 minutes sonication (see Eq. 1). Then Al/CuC energetic composite was stored in hexane for future experimentations.

$$4Al(s) + 6Cu(NH_3)_4(NO_3)_2(s) \rightarrow 2Al_2O_3(s) + 6Cu(s) + 27H_2O(g) + 6NH_3(g) + 12N_2(g) + 3N_2O(g) \quad (1)$$

2.4. Preparation of CuC/Al/CuO energetic composites

Different CuC/Al/CuO energetic composites with various mass loadings of Al/CuO nanothermite (Table 1) were prepared with an equivalence ratio of 1.2 for both Al/CuC and Al/CuO in order to investigate the effect of the nanothermite mass ratio on the pressurization and burn rate. Each composite was characterized by the weight percentage of Al/CuO nanothermite, X, ranging from 25 to 95%. Note that in a $X = 25\%$ (mixture named CuC/Al/CuO_25), the mass of Al/CuO thermite and Al/CuC is 100 mg and 300 mg, respectively.

2.5. Chemical Analysis

The morphology, particle size, agglomeration were observed by SEM using a Hitachi S-4800 (cold FEG) operating at 2.0 kV. The chemical composition of the materials was characterized using a SEIFERT XRD 3000 TT XRD with Cu-Ka radiation ($\lambda = 1.54059$ Å) fitted with a diffracted-beam graphite monochromator. The diffraction angle (2θ) was scanned from 10 to 80°.

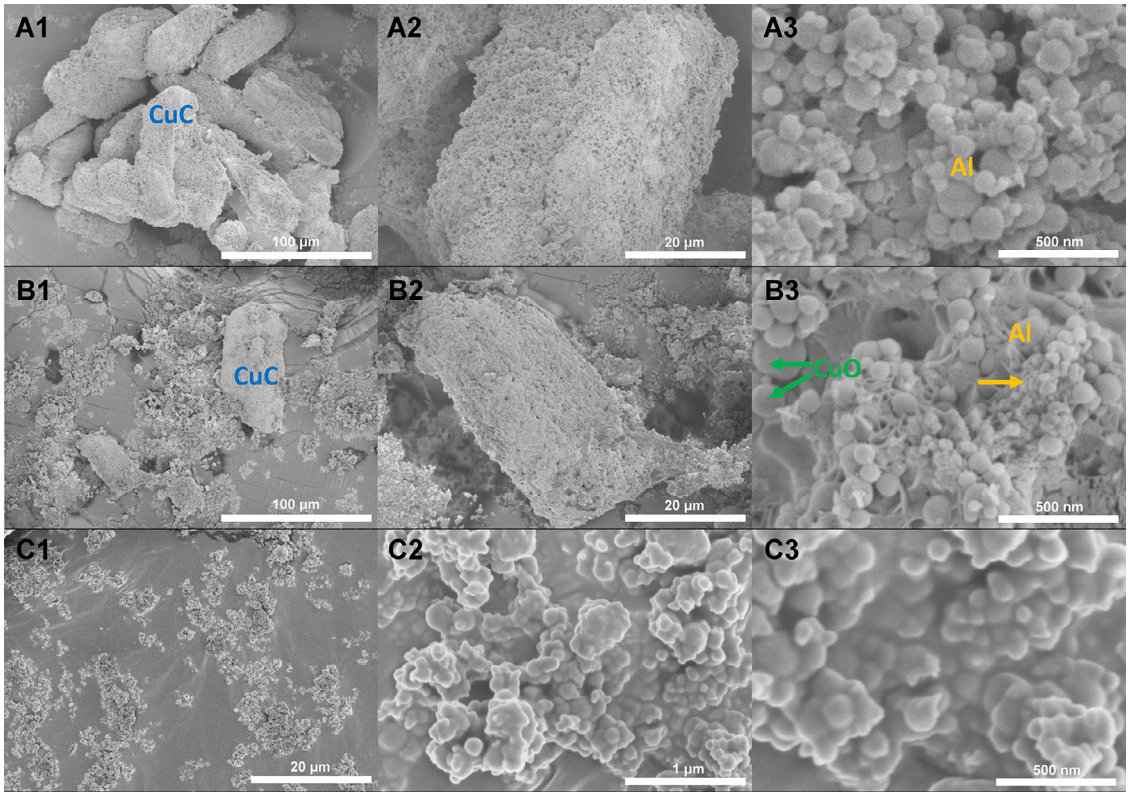

Fig. 1. SEM images of Al/CuC (A), CuC/Al/CuO_50 (B) and Al/CuO (C).

2.6. Thermal analysis

The thermal decomposition of the prepared energetic composites was characterized under a ramping heating profile at 10°C/min by: (1) Thermogravimetric/Differential Scanning Calorimetry (TGA/DSC) using a Mettler Toledo Thermogravimetric analyzer over a temperature ranging from ambient to 700°C; (2) Differential Scanning Calorimetry using a NETZSCH DSC 404 F3 Pegasus device equipped with a DSC-Cp sensor type S over a temperature ranging from ambient to 1000°C. Experiments were performed with ~5 mg of composites in platinum crucibles in Ar atmosphere (99.998% pure) at a flow rate of 20 mL/min. The traces are normalized by the mass of energetic composite material.

2.7. Thermo Gravimetric/Mass Spectroscopy

The decomposition of the energetic composites was performed by mass spectrometry (MS, equipment Pfeiffer Omnistar 1-200 amu) over a temperature range from ambient temperature to 900°C at a heating rate of 10°C/min. The MS apparatus is coupled with the TGA system described in the previous section. All measurements are performed under Argon flowing gas.

2.8. Closed bomb experiments

The pressure release is measured in a stainless steel, high pressure resistant cylindrical reactor [30]. The dimension of the reactor has a 4 mm inner diameter and is 0.7 mm long (total volume of ~9 mm^3). A stainless spacer (volume of ~25 mm^3) was placed between the reactor and the pressure sensor. For all other samples, about 13 mg of CuC/Al/CuO powders were packed in a pellet placed in the bomb which has a total volume of 25 mm^3. The packing densities of the sample filled in all pellets were calculated at around 1.5 g/cm^3. When positioned in the bomb volume, the final packing density drops down to 0.5 g/cm^3. A pressure up to 100 MPa can be measured by a high-frequency pressure transducer (Kistler 6215 type) on the back of the reactor and connected to a Kistler charge amplifier (5018 type). A schematic and a photo of the system are shown in Supplementary Information Fig. S3. For ignition, a simple NiCr wire was used.

2.9. Open burning experiments

The reaction propagation speed of composites was tested with a home-made set-up, where a rectangular holder made of polycarbonate with a trench (30 mm long, 1 mm wide and 1 mm deep) is used to support the composite material. About 25 mg of powder was loosely deposited in the trench. For ignition, a pyroMEMS chip with coating of Al/CuO nanolaminates was used to produce a flame to ignite the energetic composite [31,32]. The mean burn rate was recorded using a high-speed camera SA3 Photron able to capture the visible light perpendicular to the direction of flame propagation of the mixture, at a speed of 75,000 frames per second, with a 128×32 image resolution [33].

3. Results and Discussion

3.1. Structural characterizations

The SEM images of Al/CuC energetic materials show that the aluminum nanoparticles with an average size of 80 nm are well dispersed on the surface of copper complex rods (Fig. 1A). The SEM images taken for CuC/Al/CuO_50 energetic composite (Fig. 1B) also show a good dispersion of Al and CuO nanoparticles around CuC rods. When the nanothermite mass exceeds 50 % in CuC/Al/CuO, we notice some areas with only Al/CuO nanothermites (Fig. 1B1). As reference, SEM images of Al/CuO nanothermites are presented

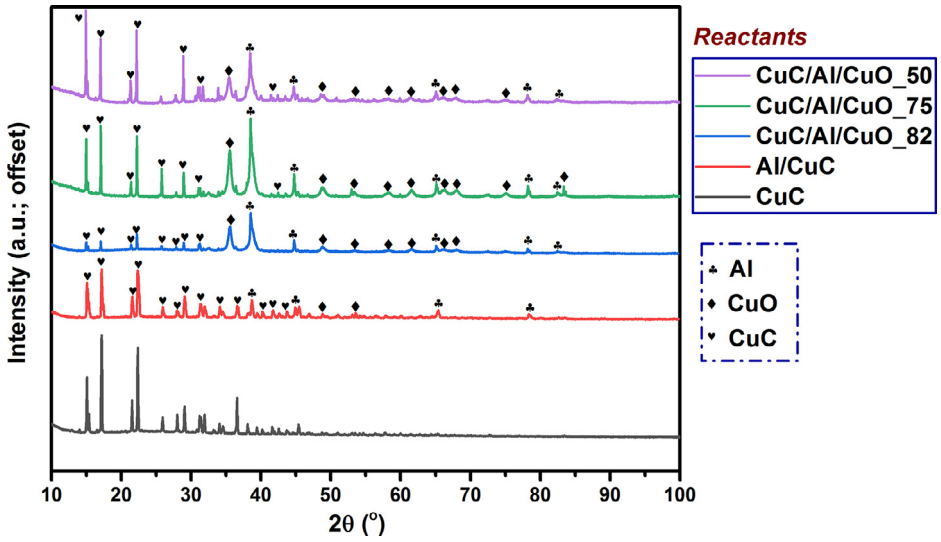

Fig. 2. XRD patterns of Al/CuC, CuC/Al/CuO_82, CuC/Al/CuO_75 and CuC/Al/CuO_50.

Table 2
Closed bomb test results of different CuC/Al/CuO composites. Each sample was tested at least three times and mean values are reported.

Sample	P_{max} (MPa)	Pressure rise rate (kPa/μs)	Packing Density (g/cm^3)
Al/CuO	1.8 ± 0.2	11 ± 0.1	0.48 ± 0.1
CuC/Al/CuO_95	3.7 ± 0.2	69 ± 6	0.44 ± 0.1
CuC/Al/CuO_90	3.5 ± 0.1	45 ± 4	0.48 ± 0.1
CuC/Al/CuO_82	4.0 ± 0.3	36 ± 10	0.48 ± 0.1
CuC/Al/CuO_75	5.9 ± 0.2	41 ± 8	0.51 ± 0.1
CuC/Al/CuO_50	No		0.51 ± 0.1
CuC/Al/CuO_25	ignition		0.50 ± 0.1

in Fig. 1C. Pictures are plotted with a greater magnification (×5 compared to other images) to distinguish Al and CuO compounds.

The XRD patterns of five different energetic composites shown in Fig. 2 indicate the compositional information: CuC, CuO and Al are detected in all samples containing nanothermite.

3.2. Pressure measurement

All prepared energetic composites were characterized in the closed bomb with a packing density kept at around 0.5 g/cm^3 for all samples (Table 2). We obtained pressure outputs (see typical temporal pressure traces plotted in Fig. 3) for all cases except for:

- Pure CuC and Al/CuC, no self-sustained reaction occurs for these two samples even with a continuous local heating through the NiCr wire.
- CuC/Al/CuO_50 and CuC/Al/CuO_25 could not be completely ignited. We suppose that the heat applied from the wire was insufficient to bring these two samples to their decomposition temperature before the wire breaks after several milliseconds. To support this theory, a lighter was used as the heat supplier and we observed violent reactions for these two mixtures after being heated. Interestingly, the moment the plastic pellet started melting, ignition happened. It implies that all CuC/Al/CuO energetic composites could be ignited as long as there was enough heat supply to the system. Thus, the ignition pathway employed in this test has its limit for these two compositions in which the CuC initiation mode dominates, i.e. heating of the whole material at the nominal decomposition temperature.

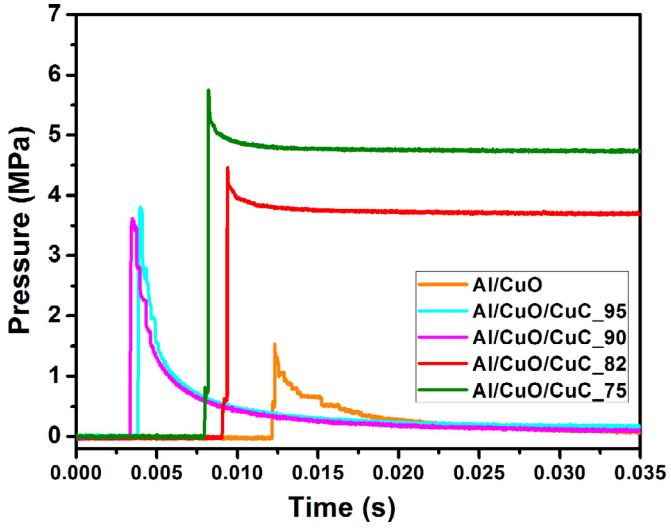

Fig. 3. Temporal pressure traces of CuC/Al/CuO energetic composites and traditional Al/CuO nanothermite as reference.

Among all other composites, the highest output pressure (Table 2) is generated by CuC/Al/CuO_75 with ~6 MPa, a value more than three times of Al/CuO taken as reference here. Note that Al/Bi_2O_3 being among the thermite couples generating the highest pressure has a peak pressure of only 1.3 times of Al/CuO [30]. Thus, the CuC/Al/CuO_75 composite, significantly outperform Al/Bi_2O_3 and Al/CuO in terms of pressure generation. Even for CuC/Al/CuO_95, where 5% by weight of Al/CuC was mixed with 95% of Al/CuO, its peak pressure still performs two times that of the traditional Al/CuO nanothermite.

In addition, the pressurization rates (the slope between two points: the peak pressure point and the point where it reaches 5% of peak pressure on pressure traces in Fig. 3) of these four CuC/Al/CuO energetic composites are much faster than that of Al/CuO. The highest value, ~70 kPa/μs, is now obtained with CuC/Al/CuO_95.

Another interesting point has to be noted from Fig. 3: it seems both CuC/Al/CuO_75 and CuC/Al/CuO_82 not only feature relatively

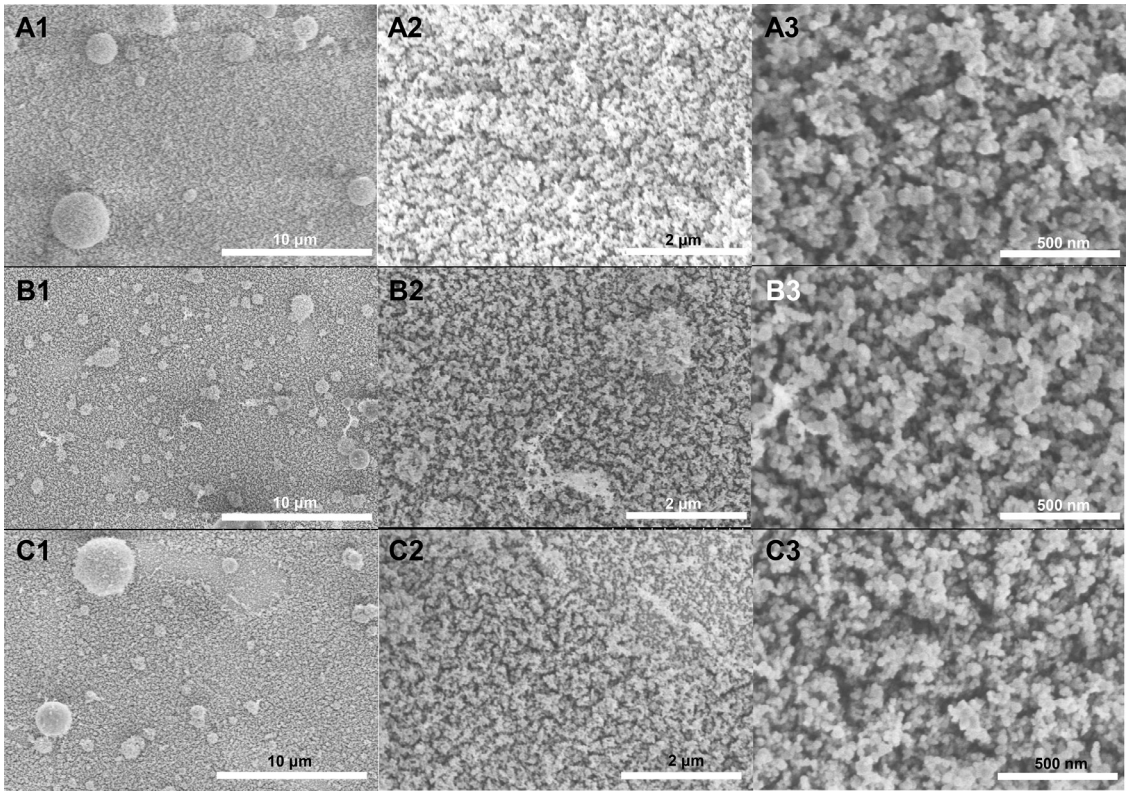

Fig. 4. SEM images of residues products from Al/CuO (A), CuC/Al/CuO_75 (B) and CuC/Al/CuO_50 (C).

Table 3
Summary of burn rates of different CuC/Al/CuO energetic composites. Each test was done at least 3 times and mean values are reported.

Samples	Burn rate (m/s)	Density (g/cm^3)
Al/CuO	36 ± 5	0.8
CuC/Al/CuO_95	40 ± 5	0.7
CuC/Al/CuO_90	64 ± 10	0.7
CuC/Al/CuO_82	79 ± 15	0.9
CuC/Al/CuO_75	141 ± 25	0.8
CuC/Al/CuO_62	135 ± 25	1.0
CuC/Al/CuO_50	3 ± 1	0.8
CuC/Al/CuO_25	No propagation	

higher peak pressure but also show much longer durations (30 ms) at maximum pressures than other samples (∼5 ms) tested in this work. It might become an attributing factor for airbag applications.

As summary of pressure tests, the optimized composition is established with 75% loading of nanothermite by weight into CuC. Also note that pressure results are obtained at very low compaction (only 0.5 g/cm^3, i.e. ∼8% TMD). These results also show that the composite can be adapted to different scenarios: relatively low peak pressure but high pressurization rate or relatively high peak pressure but low pressurization rate can be used accordingly.

3.3. Open burning experiments

The propagation speeds of all CuC/Al/CuO energetic composites were also investigated and the results are reported in Table 3. In this experiment the densities of the energetic powders inside the trench were kept at around 0.8 g/cm^3 for all tested samples.

Similar to pressure test, no propagation was observed for CuC and Al/CuC composites. Neither does CuC/Al/CuO_25. These facts indicate the weight percentage of nanothermite must reach a certain level to guarantee a self-propagated system. With 50% (by weight) addition of Al/CuO nanothermite, CuC/Al/CuO_50 demonstrated a burn rate of around 2 m/s but only 2/3 of the composite in the trench has propagated, suggesting that a bad thermal transfer within the composite might be the cause of the poor propagation behavior similar to the pressure tests (has the lowest thermal conductivity, see Supporting Information Table S1). Another possible cause might be the breakup, crystal transition and phase transition of CuC absorbing too much heat to maintain steady propagation.

All the other composites exhibit very intense burning (See snapshots in Supporting Information Fig. S4) with steady flame propagations. When the weight percentage of the nanothermite raised to 75%, the burn rate reaches the highest value among all tested samples, ∼141 m/s, 4 times higher than traditional Al/CuO nanothermite giving a burn rate of ∼36 m/s in this experimental condition. As seen in previous section, CuC/Al/CuO_75 also features the highest peak pressure generation. However, further increasing the mass loading of nanothermite decreases the burn rate dramatically rather than enhancing it. With 90% by weight of nanothermite addition, the burn rate drops to almost a half of the peak value. And it finally reaches the same burn rate as to Al/CuO when the weight percentage increases to 95%. We deduce that there is a compromise between the heat produced by the nanothermite and thermal properties varying with nanothermite percentage as the thermal conductivity increase with nanothermite loading: 56 $W.m^{-1}K^{-1}$ for CuC/Al/CuO_75 against 66 $W.m^{-1}K^{-1}$ for CuC/Al/CuO_95, thus an increase of 18% (see Supporting Information Table S1).

To fill the huge gap between a burn rate of 141 and 3 m/s, CuC/Al/CuO composite with 62% loading of nanothermite was prepared and tested afterwards. A burn rate of 137 m/s was obtained, slightly slower than that of CuC/Al/CuO_75. Similar to CuC/Al/CuO_50 and CuC/Al/CuO_25, no ignition was found in the

pressure test of CuC/Al/CuO_62. However, both CuC/Al/CuO_50 and CuC/Al/CuO_62 show steady propagations after being ignited. And CuC/Al/CuO_62 features the second fastest burn rate. It resonates with the previous discussion that ignition of the composites can only happen when enough heat is supplied in the system and a certain amount of nanothermite loading (>62%) is required for a continuous and fast propagation.

As summary, the composite featuring the fastest burn rate is those containing 75% loading of nanothermite by weight into CuC. It also features the highest-pressure output.

3.4. Post-combustion products characterization

Reaction products and residues from burn rate tests of all CuC/Al/CuO energetic composites were collected and examined by SEM. As shown in Fig. 4, giving analysis for Al/CuO, CuC/Al/CuO_75 and CuC/Al/CuO_50 samples, there are mainly two populations of product particle sizes, demonstrating the similar combustion behaviors between Al/CuO and CuC/Al/CuO composites. One has relatively larger dimension with a spherical shape and another with a dimension as small as ~50 nm but highly aggregated. EDS measurement results shown in supporting information Fig. S5-S7 indicate that the larger ones are alumina particles with a coating of copper particles, and smaller ones are copper metal aggregates (might also contain cuprous oxide particles since oxygen signal was also found in these area).

In addition, there are much less residues collected after the burning of CuC/Al/CuO energetic composites compare to Al/CuO (Fig. S8). The whole trench was covered by products with a color of dark red for Al/CuO, however, only a very thin layer of residue with a light grey were observed on the trench of other CuC/Al/CuO composites. Thus, most of the products produced from these composites are gaseous species, which is in accordance with the fact that they outperform Al/CuO in pressure generation test.

3.5. Understanding the reactions in CuC/Al/CuO energetic composites

To fully understand the combustion events of the CuC/Al/CuO energetic composites composite, all samples were thermally and chemically analyzed upon ramping ($10°C.min^{-1}$) using calorimery (TGA/DSC) coupled with time-resolved mass spectrometry.

The results of DSC experiments are presented in Fig. 5. The DSC traces of CuC and Al/CuO nanothermite are also included (Fig. 5a and 5h) as references and details on the CuC thermal decomposition (TGA/MS spectra) can be found in Supporting information (Fig. S9 and S10). The DSC trace of CuC features two endothermic peaks: first one at ~120°C might correspond to the evaporation of the physically absorbed water molecules. The second endotherm at ~210°C could be correlated to the melting of the copper complex [21] and/or the desorption of the physically absorbed ammonium. Indeed, a sharp NH_3 peak in the mass spectroscopy spectrum of CuC is observed in the same temperature range (Fig. S10). The exothermic peak located at around 270°C corresponds to the rapid decomposition of the copper complex (concomitant with mass loss seen on the TGA curve in Fig. S9) along with releases of N_2, N_2O, H_2O and NH_3 gases (detected on the MS spectra in Fig. S10). Based on the XRD analysis (Fig. 6) of the residues from the DSC experiments, the leftover powders are copper oxide particles that is the only solid product from the decomposition of copper complex. Not only the CuC acts a gas generator but it also decomposes into an oxidizer that further enables nanothermite kind of reaction with Al. Indeed, when Al nanoparticles are added into CuC (Al/CuC, Fig. 5b), a small exothermic peak appears between 500 and 600°C that is located within the Al/CuO redox reaction region proving that Al reacts with CuO originated from the decomposition of the copper complex.

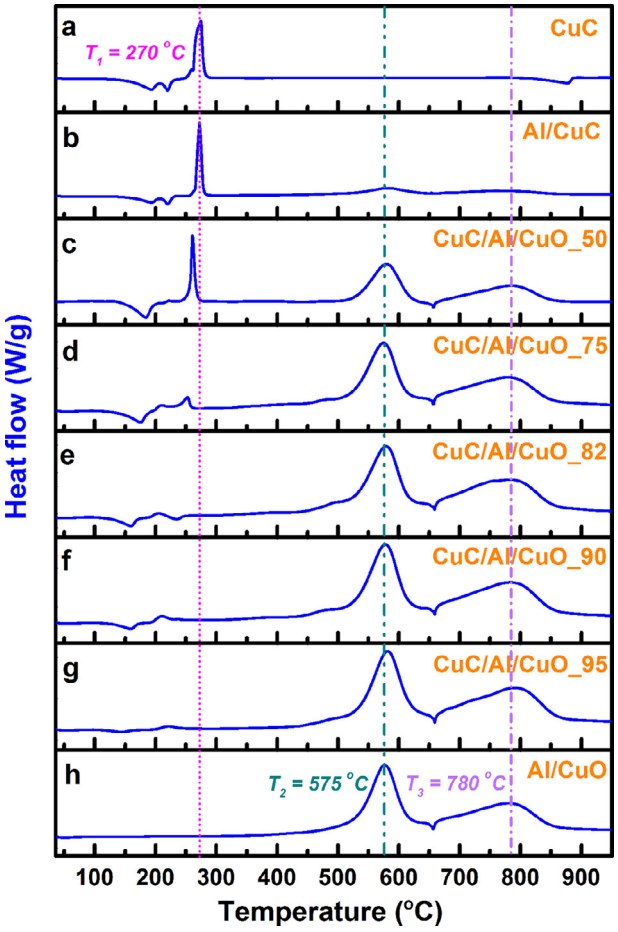

Fig. 5. DSC curves of CuC/Al/CuO energetic composites with different weight percentage of Al/CuO in argon environment.

However, the decomposition of CuC needs to be initiated first, then the decomposition product CuO could react with Al nanoparticles. Therefore, an extra heat supply is required to launch Al/CuC reaction, hence the addition of nanothermite into CuC. Different thermal behaviors are observed depending on the quantity of incorporated nanothermite. CuC/Al/CuO composites with 50 and 75% of nanothermite in weight (Fig. 5c-d) exhibit three major exothermic peaks: one at low temperature (<270°C) corresponding to the decomposition of CuC and two at high temperatures (~575 and 780°C) corresponding to the two-steps redox reaction between Al and CuO with an onset at ~530°C [34]. Several endothermic peaks are also observed corresponding to the evaporation of the physically absorbed water molecules (~180°C), the desorption of NH_3 molecules (~220°C) and the melting of CuC (~220°C) and Al (~660°C).

When the quantity of nanothermite is greater than 75% (Fig.s 3e-g), these exothermic peaks corresponding to Al/CuO redox reactions remain prominent and all located at around 575 and 780°C. However, the onset decomposition temperature of CuC is shifted toward lower temperatures: 190°C for CuC/Al/CuO_82 against 260°C for pure CuC (see detailed values in Table 4). This effect again could be associated with the added nanothermite in the system having a higher thermal conductivity compare to CuC (Table S1), thus improving the heat transfer efficiency of CuC.

A very small exothermic peak located at around 450°C is detected for all CuC/Al/CuO composites with different intensities (see arrows in supporting information Fig. S12 in close-up views). Since there is no more copper complex left at this temperature based

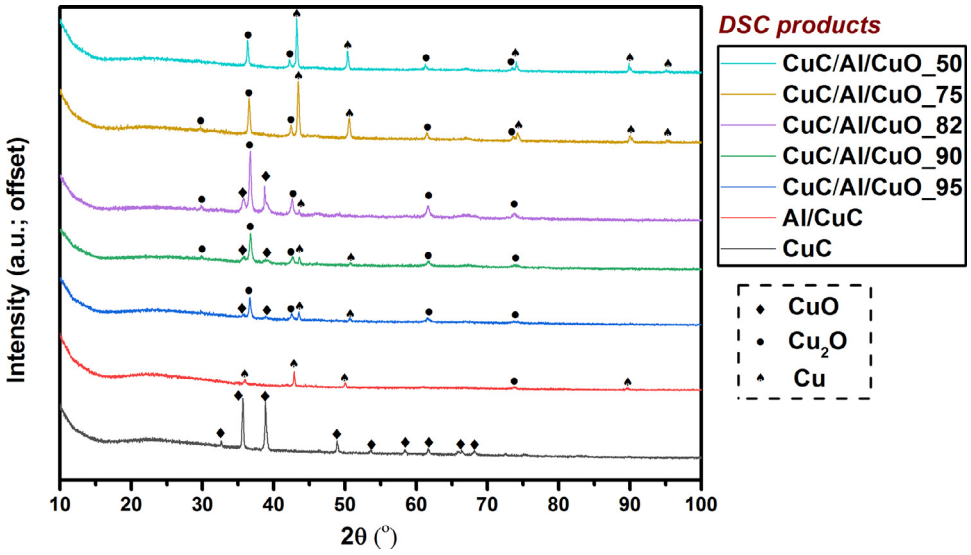

Fig. 6. XRD analysis results of residues from DSC measurements

Table 4
Summary of the experimental T_{onset} and ΔH for each reaction for pure CuCCs, Al/CuC., Al/CuO, and Al/CuO/CuC. energetic composites with different Al/CuO vs Al/CuC. mass ratios. The data are all normalized by the mass of the sample mass and have a deviation of ± 5°C. Negative values are exothermic processes.

Samples	1: Decomposition of CuC				Pre-reaction	2: Al/CuO reaction			
	T_{onset} (°C)	ΔH (J/g)	$ΔH_{th}$ (J/g)	$ΔH_{th}$- ΔH (J/g)	T_{onset} (°C)	T_{onset} (°C)	ΔH (J/g)	$ΔH_{th}$ (J/g)	$ΔH_{th}$-ΔH (J/g)
CuC	257	−795	–	–	–	–	–	–	–
Al/CuO	–	–	–	–	–	530	−4071	4072[a]	–
Al/CuC	265	−1118	–	–	–	534	−1453	–	–
CuC/Al/CuO_50	257	−253	−358	105	443	531	−2483	−2763	280
CuC/Al/CuO_75	240	−57	−179	122	451	527	−3196	−3417	222
CuC/Al/CuO_82	192	−16	−129	113	456	532	−2540	−3601	1061
CuC/Al/CuO_90	195	−28	−72	44	445	533	−2390	−3810	1422
CuC/Al/CuO_95	200	−15	−36	21	445	532	−2777	−3941	1164

[a] theoretical ΔH from a previous publication [30].

on the TGA/DSC/MS results of copper complex and Al/CuC, and no such peak is observed in Al/CuO or Al/CuC, this exothermic peak is likely to be an outcome from a pre-reaction between aluminum and copper oxides (that include not only commercial CuO but also CuO originated from CuC).

All information derived from DSC analysis are summarized in Table 4 with the corresponding heats of reaction (ΔH). Since the peak corresponding to the decomposition of CuC (270°C in Fig. 3a) is shifted to lower temperatures in DSC curves of other CuC/Al/CuO composites, the total heat of reaction for the decomposition of CuC is calculated by integrating the corresponding exothermic peak. A temperature range from 400 to 900°C is used for the calculation of the heat of reaction of Al/CuO. The data are all normalized by the sample mass.

First, the decomposition step of CuC remains exothermic with or without the presence of nanothermites in the system. However, the intensity of this exothermic peak, ΔH, decreases dramatically with increasing weight percentage of nanothermite in the system. Indeed, it is 250 J/g and only 15 J/g for 50% and 95% of Al/CuO mixed with Al/CuC, respectively. This is in accordance with calculations shown in Table 4, where the corresponding calculated ΔH ($ΔH_{th}$) of the decomposition of CuC is decreasing with the increasing of the incorporated nanothermite due to the decrease of CuC weight percentage inside composites.

Second, we note that all experimental ΔH values are much lower than the calculated ones ($ΔH_{th}$). Based on the calculation results on heat of reaction of Al/CuO of all composites listed in Table 4, CuC/Al/CuO_95 was expected to be the one that generates the highest energy output. However, the maximum heat of reaction is experimentally reached when 75% of Al/CuO nanothermite is incorporated into the Al/CuC system. It is also noted the CuC/Al/CuO_75 features the smallest difference between experimental and calculated ΔH. We suggest two possible reasons:

(1) Both aluminum and copper oxide being much better heat conductors than CuC, one reason would be simply that the heat produced by the CuC decomposition is quickly absorbed and evacuated by the nanothermite present in the system. The thermal conductivity of the composite improves with increasing nanothermite loading (See Table S1 for detailed information regarding thermal properties of each composites).
(2) The second reaction (Al/CuO) can be simply the incompleteness of the reactions. Considering CuC has already fully decomposed into CuO at 400 °C, its effect can be excluded here. Since all experiments were conducted under the same conditions, human/machine errors should be theoretically identical. Thus, the divergence between calculated and experimental results could be resulted from the mixture itself at this temperature range (>400 °C). Therefore, residues from DSC measurement were collected and examined by XRD method and the results are presented in Fig. 6. All data is summarized in supporting information Table S3. The residues collected from Al/CuC and CuC/Al/CuO composites, after being heated to such temperature, contain a mixture of copper metal (Cu), cuprous oxide (Cu_2O), and/or copper oxide, which in-

dicates an incomplete redox reaction between aluminum and copper oxide originated from the thermite and decomposition of CuC. By analyzing each curve in Fig. 6, the XRD results do support this theory based on the following evidence. Firstly, both CuC/Al/CuO_75 and CuC/Al/CuO_50 have five XRD peaks corresponding to the presence of copper metal (labeled as spade), three more than the other CuC/Al/CuO composites. And the peak intensities of CuC/Al/CuO_75 and CuC/Al/CuO_50 are much stronger, indicating more copper products and therefore higher reaction completion. Secondly, Cu_2O signals were found in all CuC/Al/CuO composites, indicating incomplete Al/CuO reactions. Thirdly, no signal related to CuO was detected in the residues of CuC/Al/CuO_75 and CuC/Al/CuO_50, however, it was found in all the other CuC/Al/CuO residues implies serious incompletions. Hence, it is reasonable to say that the degree of completion of Al/CuO redox reaction in CuC/Al/CuO_75 and CuC/Al/CuO_50 is much higher than the other CuC/Al/CuO composites. Due to the incompletion, all experimental ΔH values are lower than the corresponding ΔH_{th}. And a much lower ΔH value was experimentally obtained for CuC/Al/CuO_82, CuC/Al/CuO_90 and CuC/Al/CuO_95 because of their significant low degrees of completion. In accordance with the theoretical results, CuC/Al/CuO_75 shows a higher experimental ΔH than CuC/Al/CuO_50 while suffering the same amount of ΔH deviation. Moreover, CuC/Al/CuO_75 does outperform all the others in gas generation and burning rate experiments according to section 3.2 and 3.3.

Finally, mass spectrometry analyses of all prepared energetic composites upon heating (with a heating rate of $10°C.min^{-1}$) under argon atmosphere reveal that mass losses (starting at ~250°C and finishing before 300°C) are accompanied with the release of different species (N_2, N_2O, H_2O and NH_3 gases). As shown in Fig. 7 (MS spectra for CuC, Al/CuC and CuC/Al/CuO_50 at ambient temperature and several temperatures around 100, 220, 240, 260, 270, 280 and 300°C) the type of gaseous species are the same whatever the quantity of Al/CuO incorporated into the CuC material. In accordance with the TGA/DSC results, these energetic composites materials begin to release N_2O and N_2 at around 250°C and finish before 300°C. For all three cases, water molecules are detected from the beginning to the end, indicating the presence of water molecules inside the mass spectrometer chamber. Due to this reason, it is difficult to differentiate the source of the H_2O signals. Looking at intensities of NH_3 in all three graphs, a common path was noticed that NH_3 reaches its peak release at a temperature between 220-250 °C, earlier than the peak release of N_2O and N_2, indicating desorption of NH_3 happens prior to the full decomposition of CuC that was verified previously by DSC results (Fig. 5). The fact that NH_3 peaks are shown in all temperature range implies that there are lots of NH_3 molecules attached on/in the composite materials (probably on CuC) considering excess ammonium was used during the synthesis of CuC. In fact, the signal intensities of NH_3 and H_2O are stronger than the other two species according to the MS spectra of CuC shown in supporting information Fig. S5.

Altogether these DSC + MS results experimentally demonstrate that the presence of CuC does not affect the chemical nanothermite reaction although it significantly influences the burning of the composite. We deduce that at low heating rates the CuC decomposition and heat from thermite reaction work sequentially based on a 3 sequential reactions chemistry summarized below:

Peak at 270°C:

$$2Cu(NH_3)_4(NO_3)_2(s) \rightarrow 2CuO(s) + 9H_2O(g) + 2NH_3(g) + 4N_2(g) + N_2O(g) \quad (2)$$

Peak at 575°C:

$$2Al\ (s) + 6CuO\ (s) \rightarrow Al_2O_3(s) + 3Cu_2O(s) \quad (3)$$

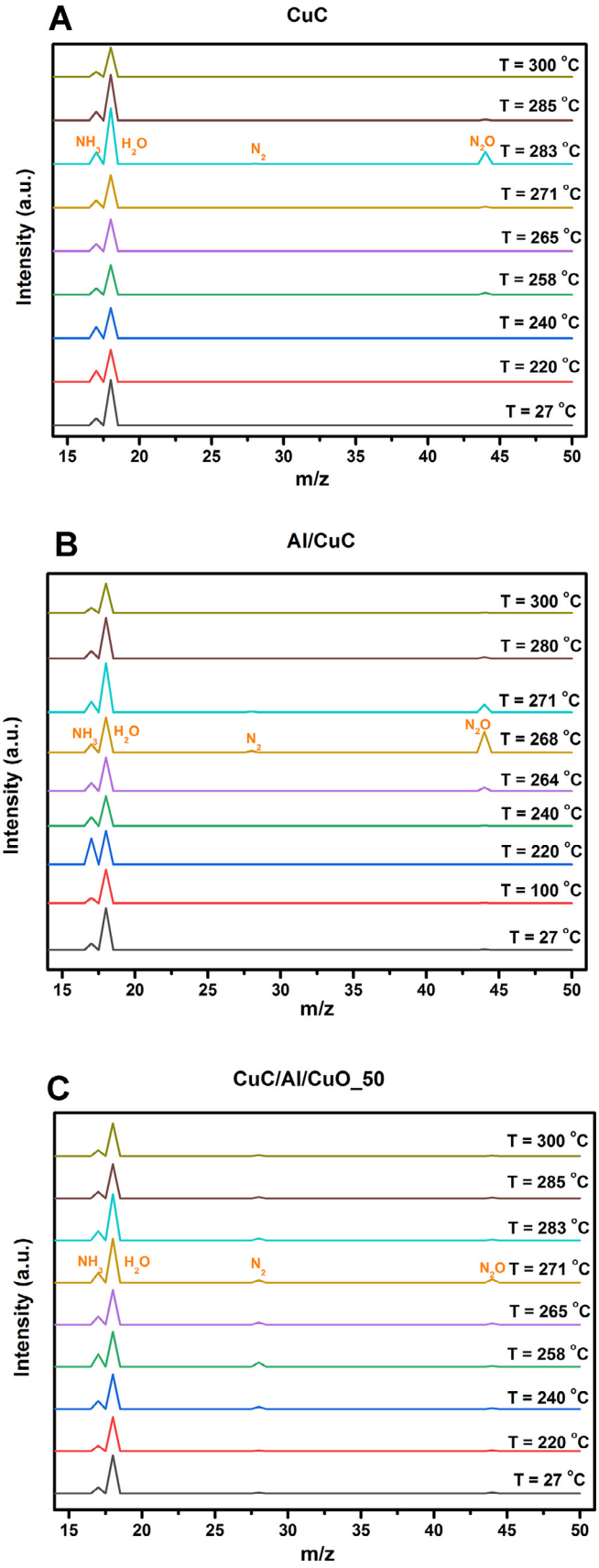

Fig. 7. Mass spectra of CuC, Al/CuC and CuC/Al/CuO_50 energetic composites at various temperatures in argon environment.

Peak at 780°C:

$$2Al\ (s) + 3Cu_2O\ (s) \rightarrow Al_2O_3(s) + 6Cu(s) \quad (4)$$

Different from DSC experiment where event lasts more than hours, in close bomb and burn rate experiments, the combustion event finishes on a time scale of milliseconds and occurs at a very high heating rate [35]. Therefore, combine with the results from closed bomb and burn rate experiments, here we suggest that at a high heating rate, CuC/Al/CuO composites likely undergo a different sequential reaction: (1) Al/CuO ignites locally and propagates; (2) heat generated by Al/CuO reaction promotes the decomposition of CuC; (3) CuO product from CuC decomposition either participates in Al/CuO reaction or is splashed out by gaseous products before contacting with Al.

4. Conclusions

In this work, for the first time, a coordination complex $Cu(NH_3)_4(NO_3)_2$, was mixed with a thermite to build a novel gas generator system with versatile and exquisite properties in term of gas generation and associated rising time. The decomposition temperature of CuC was located at around 270°C according to its DSC result. NH_3, N_2O and N_2 were identified to be the gaseous products from its decomposition. Since without external heat, CuC cannot initiate and sustain its decomposition, Al/CuO nanothermite was incorporated to act as the complementary heat source upon initiation of the whole material. The optimized weight percentage of Al/CuO nanothermite allowing the self-sustained decomposition of CuC, faster burn rate and maximum boost on peak pressure is 75%. These new energetic composites feature peak pressure of 12 MPa/g.cm^3, which is much higher that traditional Al/CuO nanothermite. It has to be noted that the incorporation of nanothermite into the complex lower the decomposition temperature of CuC to 190°C instead of 260°C. We also experimentally proved that by simply tuning the weight percentage of incorporated Al/CuO nanothermite, different heat of reactions, pressure outputs and burn rates can be obtained. Analysis of residues showed that the majority of the combustion products is in the gas phase considering only a thin layer of soft grey product left after.

Author contributions

T. Wu prepared all samples and performed all characterization measurements. F. Sevely assisted T. Wu in experimental set-up designs and close bomb and open burning experiments. C. Tenailleau performed XRD measurements. B. Julien assisted T. Wu in close bomb experiment. J. Cure assisted T. Wu in XRD and MS analysis. C. Rossi provided support for the manuscript preparation and supervised the research.

The manuscript was written through contributions of all authors. All authors have given approval to the final version of the manuscript.

Funding Sources

C. Rossi received funding from the European Research Council (ERC) under the European Union's Horizon 2020 research and innovation programme (grant agreement No 832889 - PyroSafe).

Competing financial interests

The authors declare no competing financial interests.

Acknowledgment

The authors acknowledge support from the European Research Council (H2020 Excellent Science) Researcher Award (grant 832889 – PyroSafe) and the Occitanie Region / European Union for their FEDER support (THERMIE grant). The authors also thank Mohammed Aizane from CIRIMAT for his assistance in TGA/MS analysis as well as Dr. Bruno Chaudret, from LPCNO, for his initial idea to explore Werner Complex as energetic material in 2008 [28].

Supplementary materials

Supplementary material associated with this article can be found, in the online version, at doi:10.1016/j.combustflame.2020.05.022.

References

[1] R.N. Khouzam, S. Al-Mawed, V. Farah, A. Mizeracki, Next-generation airbags and the possibility of negative outcomes due to thoracic injury, Can. J. Cardiol. 30 (2014) 396–404.
[2] A. Shaout, C.A. Mallon, Automotive airbag technology: past, present and future, Int. J. Comput. Appl. T. 13 (2000) 159–171.
[3] Air Bags. https://www.nhtsa.gov/equipment/air-bags.
[4] L. Shamo, This personal airbag could help protect the elderly from hip injuries. https://www.businessinsider.com/hipair-inflates-prevents-hip-injuries-elderly-wearable-personal-airbag-2018-1?IR=T.
[5] Q. Zhang, H.Q. Li, Y.K. Ning, D. Liang, G.R. Zhao, Design and realization of a wearable hip-airbag system for fall protection, Appl. Mech. Mater. 461 (2014) 667–674.
[6] https://www.abs-airbag.com/fr/systeme-abs.html.
[7] G. Shi, C.S. Chan, W.J. Li, K. Leung, Y. Zou, Y. Jin, Mobile human airbag system for fall protection using mems sensors and embedded SVM classifier, IEEE Sens. J. 9 (2009) 495–503.
[8] C.S. Chan, G. Shi, Y. Luo, G. Zhang, W.J. Li, P.H.W. Leong, K. Leung, A human-airbag system for hip protection using mems motion sensors: experimental feasibility results, International Conference on Mechatronics and Automation (2006), pp. 831–836. 25-28 June.
[9] R. Nayak, R. Padhye, K. Sinnappoo, L. Arnold, B.K. Behera, Airbags, Textile Progress, 45, 2013, pp. 209–301.
[10] H. Potvin, M.H. Back, A study of the decomposition of sodium azide using differential thermal analysis, Can. J. Chem. 51 (1973) 183–186.
[11] H.S. Kim, J.H. Kim, J.H. Ku, M.H. Cho, J.K. Cha, J.M. Kim, H.W. Lee, S.H. Kim, Effects of metal oxide nanoparticles on combustion and gas-generating performance of NaN_3/Al composite powders ignited using a microhotplate platform, Adv. Powder Technol (2020) 1023–1031.
[12] A. Surendran Lathika, S. Suthangathan Paramashivan, B. Karuppudaiyar Ramasamy, S. Mahadevan, Impact of fuel/oxidizer ratio of NaN_3 and KNO_3 airbag gas generants on toxic emission and performance, Process Saf. Environ. 133 (2020) 348–357.
[13] K.R. Olson, I.B. Anderson, N.L. Benowitz, P.D. Blanc, R.F. Clark, T.E. Kearney, S.Y. Kim-Katz, A.H.B. Wu, Poisoning & drug overdose, seventh edition, in: B. Belval, C. Naglieri (Eds.), Poisoning & drug overdose, The McGraw-Hill Companies Inc, the United States of America, 2018.
[14] S. Zeuner, A. Hofmann, R. Schropp, K.-H. Rödig, Guanidine-thermite igniter composition for use in gas generators, TRW Airbag Systems GmbH (2000) US6599380B2.
[15] P.S. Khandhadia, S.P. Burns, G.K. Williams, High gas yield non-azide gas generants, 1998, US6210505.
[16] U.S. EPA., Provisional peer-reviewed toxicity values for guanidine chloride, U.S. Environmental Protection Agency, Washington, DC, 2014.
[17] H. Tabuchi, Airbag Compound Has Vexed Takata for Years. https://www.nytimes.com/2014/12/10/business/compound-in-takata-airbags-is-inquirys-focus.html.
[18] A. Lafrance, How Airbags Are Supposed to Work. https://www.theatlantic.com/technology/archive/2015/06/airbags/396854/.
[19] T.M. Southern, W.W. Wendlandt, The thermal decomposition of metal complexes—XX: Some amine copper(II) nitrate complexes, J. Inorg. Nucl. Ch. 32 (1970) 3783–3792.
[20] S. Mathew, C.G.R. Nair, K.N. Ninan, Thermal decomposition studies on amine complexes of copper(II) nitrate in solid state, B. Chem. Soc. Jpn. 64 (1991) 3207–3209.
[21] M. Künzel, J. Selesovsky, R. Matyáš, Characterization of tetraamminecopper salts, 18th New Trends in Research of Energetic Materials, Pardubice, Czech Republic (2015), pp. 664–669.
[22] M. Künzel, O. Vodochodský, R. Matyáš, Z. Jalový, J. Pachman, J. Maixner, Tetraamminecopper(II) nitrate and its effects on ammonium nitrate(V) central european, J. Energ. Mater. 14 (2017) 169–183.
[23] M. Liszka-Skoczylas, E. Mikuli, J. Szklarzewicz, J. Hetmańczyk, Thermal behaviour, phase transition and molecular motions in $[Co(NH_3)_6](NO_3)_2$, Thermochim. Acta 496 (2009) 38–44.
[24] W.W. Wendlandt, J.P. Smith, Thermal decomposition of metal complexes—VI some ammine cobalt (II) complexes, J. Inorg. Nucl. Ch. 25 (1963) 985–993.
[25] A. Migdał-Mikuli, E. Mikuli, R. Dziembaj, D. Majda, Ł. Hetmańczyk, Thermal decomposition of $[Mg(NH_3)_6](NO_3)_2$, $[Ni(NH_3)_6](NO_3)_2$ and $[Ni(ND_3)_6](NO_3)_2$, Thermochim. Acta 419 (2004) 223–229.

[26] J.M. Janik, E. Mikuli, A. Migdal-Mikuli, M. Rachwalska, T. Stanek, J.A. Janik, K. Otnes, I. Svare, Calorimetry, proton magnetic resonance and neutron quasielastic scattering studies of $[Mg(H_2O)_6](NO_3)_2$, Phys. Scripta 28 (1983) 569–572.
[27] E. Mikuli, M. Liszka, M. Molenda, Thermal decomposition of $[Cd(NH_3)_6](NO_3)_2$, J. Therm. Anal. Calorim. 89 (2007) 573–578.
[28] C. Pradère, S. Suhard, L. Vendier, G. Jacob, B. Chaudret, S. Sabo-Etienne, Heterometallic werner complexes as energetic materials, Dalton. T. 20 (2008) 2725–2731.
[29] G.K. Lund, J.C. Hinshaw, D.W. Doll, R.J. Blau, Metal complexes for use as gas generants 1997, WO1998006486A2.
[30] L. Glavier, G. Taton, J.-M. Ducéré, V. Baijot, S. Pinon, T. Calais, A. Estève, M. Djafari Rouhani, C. Rossi, Nanoenergetics as pressure generator for nontoxic impact primers: Comparison of Al/Bi_2O_3, Al/CuO, Al/MoO_3 nanothermites and Al/PTFE, Combust. Flame 162 (2015) 1813–1820.
[31] A. Nicollet, L. Salvagnac, V. Baijot, A. Estève, C. Rossi, Fast circuit breaker based on integration of Al/CuO nanothermites, Sensor Actuat. A-Phys. 273 (2018) 249–255.
[32] C. Rossi, Engineering of Al/CuO reactive multilayer thin films for tunable initiation and actuation, propellants, explosives, Pyrot. 44 (2019) 94–108.
[33] B. Julien, J. Cure, L. Salvagnac, C. Josse, A. Esteve, C. Rossi, Integration of gold nanoparticles to modulate the ignitability of nanothermite films, ACS Appl. Mater. 3 (2020) 2562–2572.
[34] I. Abdallah, J. Zapata, G. Lahiner, B. Warot-Fonrose, J. Cure, Y. Chabal, A. Esteve, C. Rossi, Structure and chemical characterization at the atomic level of reactions in Al/CuO multilayers, ACS Appl. Ener. Mater. 1 (2018) 1762–1770.
[35] T. Wu, X. Wang, P.Y. Zavalij, J.B. Delisio, H. Wang, M.R. Zachariah, Performance of iodine oxides/iodic acids as oxidizers in thermite systems, Combust. Flame 191 (2018) 335–342.